Solid–Vapour Reactions of Cholic Acid and Methyl Cholate with Acetonitrile: Structures and Reaction Kinetics

Janet L. Scott
Department of Chemistry, University of Cape Town, Rondebosch, 7700, South Africa

Both cholic acid and methyl cholate react to form 1:1 inclusion complexes with acetonitrile either by crystallisation from solution or by solid–vapour reaction. Crystal structures of cholic acid·acetonitrile, methyl cholate·acetonitrile and methyl cholate alone are presented and analysed for strong interactions in an attempt to reconcile the structures of the reactants and products to kinetic data derived from absorption and desorption reactions. Relative rates of absorption and estimates of kinetic parameters, E_a and ln A, for the desorption reactions are presented.

Inclusion compounds of organic hosts and guests are usually produced by recrystallisation either from solutions of the host in liquid guest or host and guest dissolved in a common solvent. In a few cases inclusion compounds may be formed in the solid state by contact of solid host and solid guest.[1,2] It is however possible to form inclusion compounds with certain host–guest systems by solid/gas reaction achieved by exposure of the solid host material to vapours of the guest. Such reactions are relatively well known with inorganic hosts such as zeolites[3,4] and Werner clathrates[5] but there are few examples of solid-vapour reactions with organic host molecules.

The reaction between host and guest, which may be represented: $xH_{(s)} + yG_{(g)} = H_xG_{y(s)}$, proceeds with change of phase from that of the host alone to the clathrate phase with concomitant change in molar volume which may be monitored to provide a measure of extent of reaction. Recently a volumetric method for following the rate of intercalation of liquid guests into layered hosts has been reported.[6] Compounds that absorb guest vapours, with formation of a new crystalline phase, are potentially useful as chemical sensors for determination of atmospheric concentrations of solvents[7] or as stationary phases in gas chromatography. Adsorption of the guest and formation of the host:guest complex results in a mass increase which may be detected with the aid of a microbalance and used to monitor the rate and extent of the reaction.

Study of reaction kinetics aids elucidation of reaction mechanisms. The formation of the 1:2 (host:guest) inclusion compounds with acetone guest and diol hosts such as *trans*-9,10-dihydroxy-9,10-diphenyl-9,10-dihydroanthracene[8] and 1,1,6,6-tetraphenylhexa-2,4-diyne-1,6-diol[9] by vapour–solid reaction have been studied.

Cholic acid (CA) (3α,7α,12α-trihydroxy-5β-cholan-24-oic acid) and its O(28) methyl ester, methyl cholate (MC), have been shown to act as host molecules forming inclusion compounds with a variety of small organic guest molecules. Both form inclusion compounds with the lower alcohols,[10–12] in which host and guest are extensively hydrogen bonded. Cholic acid forms tubulate clathrates with a wide variety of chemically different guest molecules such as benzene[13] and benzene derivatives,[14–16] aliphatic esters,[17] ketones[18] and lactones.[19]

We report the formation of 1:1 (host:guest) inclusion compounds of CA and MC with acetonitrile by reaction of the solid host with acetonitrile vapour. The product phases are characterised and found to be indistinguishable from the 1:1 host:guest complexes of CA and MC with acetonitrile formed in the usual manner from solution. Crystal structures of the inclusion compounds as well as that of the MC host with no included guests [MC(α)] are presented and the kinetics of guest absorption and desorption investigated.

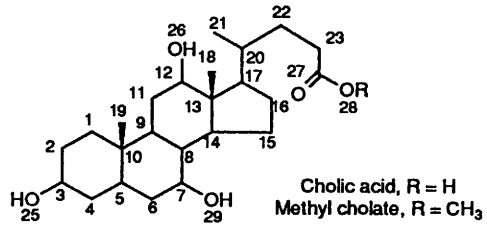

Experimental

Single crystals of the inclusion compounds were grown by slow evaporation from solutions of the host in acetonitrile or in a mixture of acetonitrile and acetone. The crystals grew as colourless, tabular prisms in the case of MC·acetonitrile (MCCN) and as colourless needles in the case of CA·acetonitrile (CACN). Single crystals of the methyl cholate host without guest, [MC(α)], were grown serendipitously from a solution of MC in *n*-butanol and tetrahydrofuran. Selected crystals were sealed in Lindemann capillary tubes as (although both inclusion complexes are remarkably stable with respect to desorption of the guest) crystals of these compounds are readily attacked by vapours from the materials used to secure the crystals to glass fibres. Preliminary cell parameters were obtained photographically and intensity data were collected on an Enraf-Nonius CAD4 diffractometer at 294 K using graphite monochromated Mo-Kα radiation (λ = 0.7107 Å) and the ω–2θ scan mode. During data collection three reference reflections were monitored periodically to check crystal stability. The data were corrected for Lorentz-polarisation effects. Refined unit cell parameters were obtained by least-squares analysis of 24 reflections measured on the diffractometer in the range $16° < \theta < 17°$. Crystal data and other experimental details are given in Table 1.

Structure Solution and Refinement.—Both inclusion compound structures were solved by direct methods using the program SHELX-86[20] and refined by full-matrix least-squares refinement using the program SHELX-76.[21] The weighting scheme employed was with $w = [\sigma^2(F) + gF_o^2]^{-1}$ values of g chosen to ensure constant distributions of $\langle w(|F_o| - |F_c|)^2 \rangle$ with respect to $\sin\theta$ and $(F_o/F_{max})^{\frac{1}{2}}$. The y coordinate of one carbon atom of the host molecule was fixed in each case to define the origin in the polar space group $P2_1$. In the final models all non-hydrogen atoms were refined anisotropically.

Table 1 Crystal data, experimental and refinement parameters

Compound	CACN	MCCN	MC(α)
Crystal data			
Molecular formula	$C_{24}H_{40}O_5 \cdot C_2H_3N$	$C_{25}H_{42}O_5 \cdot C_2H_3N$	$C_{25}H_{42}O_5$
Molecular weight/g mol^{-1}	449.63	463.66	422.61
Space group	$P2_1$	$P2_1$	$P2_12_12$
a/Å	9.645(2)	9.891(3)	42.387(2)
b/Å	8.401(1)	8.390(2)	14.563(3)
c/Å	15.747(4)	16.024(4)	7.660(1)
α/°	90.0	90.0	90.0
β/°	101.01(2)	99.10(2)	90.0
γ/°	90.0	90.0	90.0
V/Å^3	1252.5(5)	1313.0(6)	4728(1)
Z	2	2	8
D_c/g cm^{-3}	1.192	1.173	1.187
μ(Mo-Kα)/cm^{-1}	0.76	0.74	0.81
F/000	492	508	1856
Data collection			
Crystal dimensions	0.4 × 0.4 × 0.35	0.5 × 0.5 × 0.4	0.1 × 0.2 × 0.25
Range scanned θ/°	1–25	1–25	1–25
Range of indices h,k,l	±11, +10, +18	±11, +9, +19	+50, −17, +9
Reflections for lattice parameters no., θ range/°	24, 16–17	24, 16–17	24, 16–17
Instability of standard reflections (%)	0.4	−1.8	−2.1
Number of reflections collected (unique)	2449	2561	4714
Number of reflections observed with $I_{rel} > 2\sigma I_{rel}$	1804	1894	2015
Final refinement			
No. of reflections	1774	1894	4714[a]
Number of parameters	320	310	541
R	0.0409	0.0489	0.0667
wR	0.0395	0.0520	*a*
g	0.0001	0.00	
S	1.75	3.27	*a*
Max. height in difference Fourier map/eA^{-3}	0.22	0.43	0.45
Min. height in difference Fourier map/eA^{-3}	−0.36	−0.31	−0.33

[a] Refined on F^2 using 4714 unique reflections with 8 restraints and 541 least-squares parameters resulting in GooF = 1.018 and R_1 = 0.0667, wR_2 = 0.1629 for reflections with $I > 2\sigma(I)$ and R_1 = 0.2394, wR_2 = 0.2343 for all data

Methine, methylene and methyl hydrogen atoms were placed in geometrically generated positions and refined with positional parameters riding on the host atom and with each type tied to a common temperature factor. Host hydroxy hydrogen atoms were located in electron density difference maps and refined with O–H bond lengths restraints.

The structure of MC(α) was solved using the program SHELX-86[20] and refined by full-matrix least squares refinement on F^2 using the program SHELXL-93.[22] The weighting scheme employed was $w = [\sigma^2(F_o^2) + (0.1085P)^2 + 1.2858P]^{-1}$, where $P = [\text{Max}(0, F_o^2) + 2F_c^2]/3$. In the final model all non-hydrogen atoms except the oxygen and methyl carbon atoms of the terminal ester group were refined anisotropically. Methine, methylene and methyl hydrogen atoms were placed in geometrically generated positions and refined with positional parameters riding on the host atom. Each type of hydrogen atom was tied to a common temperature factor, which was allowed to refine. Host hydroxy hydrogen atoms were located in electron density difference maps and refined with O–H bond length restraints. There are two independent MC molecules in the asymmetric unit of the MC(α) structure and these are labelled molecules A and B.

Final fractional atomic coordinates, temperature factors, bond lengths and bond angles have been deposited at the Cambridge Crystallographic Data Centre.†

† For full details of the deposition scheme, see 'Instructions for Authors (1995),' *J. Chem. Soc., Perkin Trans. 2*, 1995, Issue 1.

Thermal Analysis.—Differential Scanning Calorimetry, (DSC) and Thermal Gravimetry, (TG), were performed on a Perkin-Elmer PC7 system.

Rising temperature thermal analysis. Crystals of the inclusion compounds were removed from their mother liquor, blotted dry on filter paper and lightly crushed before analysis. Sample masses in the range 1–5 mg were analysed in the temperature range 30–230 °C at a heating rate of 20 °C min^{-1} with dry nitrogen purge gas at a flow rate of 40 cm^3 min^{-1}.

Kinetics. Crystals of CACN and MCCN were grown as for X-ray diffractometry and were filtered from the mother liquor, crushed and sieved. The fractions with particle size 212–250 μm were retained and the powders kept under an atmosphere of acetonitrile to prevent desorption of the guest over a period of days. The desorption reactions were carried out under isothermal thermogravimetric conditions at different temperatures in the range 78–112 °C for CACN and 85–100 °C for MCCN. The resultant weight loss percentage *versus* time curves were converted to extent of reaction (α) *versus* time curves, which were fitted to one of the common rate law equations.[23] The best fit was deemed to be that which most nearly approached linearity over the largest α range (0.05–0.95 in both cases). Values of k thus obtained were used to produce Arrhenius plots for estimation of the activation energies.

Gas/Solid Absorption.—The rate of acetonitrile vapour absorption by dried, powdered host compounds was measured using an apparatus designed to allow automatic monitoring of mass increase under controlled atmospheres at constant temperatures as described by Barbour *et al.*[24] Crystalline

Table 2 Torsion angles defining side-chain configuration of the host steroid.

				MC(α)	
		CACN	MCCN	A	B
τ_1	C(13)–C(17)–C(20)–C(22)	−177.2(4)	−178.4(5)	−178.4(5)	174.7(7)
τ_2	C(17)–C(20)–C(20)–C(22)	−164.1(4)	−169.8(6)	60.0(10)	−165.4(8)
τ_3	C(20)–C(22)–C(23)–C(24)	−172.5(4)	−175.0(6)	170.7(10)	−175.1(9)
τ_4	C(22)–C(23)–C(24)–O(27)	142.6(5)	−6.1(12)	−14.4(18)	−133.9(13)
τ_5	C(22)–C(23)–C(24)–O(28)	−37.7(6)	174.8(6)	163.8(12)	48.4(14)

samples recrystallised from acetone–acetonitrile mixtures were dried at elevated temperatures *in vacuo* until all solvent was desorbed as measured by zero weight loss on TG analysis. This material [which in each case was shown to be identical to the (α) phase by XRD analysis] was crushed and sieved and the 212–250 μm fraction retained. Weighed samples of the dried host materials were placed in the reaction chamber which was evacuated and acetonitrile liquid introduced. A small pool of acetonitrile was maintained in the bottom of the reaction vessel to ensure constant vapour pressure of the guest and the subsequent gain in mass of the sample monitored continuously. Weight gain *versus* time isotherms were obtained and transformed to α *versus* time curves.

X-Ray Diffraction.—Powder diffraction spectra of the inclusion compounds formed both by gas–solid reaction or crystallisation and of the desolvated materials were recorded at 294 K using the continuous scan mode and Cu-Kα radiation. Crystalline samples were crushed to approximate the size distribution of the powder samples and the spectrum recorded over the 2θ range 6–36°.

Results and Discussion

1 : 1 Host : guest stoichiometries were confirmed by weight loss on heating as measured by TG. The experimental and calculated weight losses were 9.15 (calc. 9.13%) for CACN and 8.86 (calc. 8.85%) for MCCN and site occupancy factors of unity were thus employed in refinement of guest atoms. Anisotropic displacement parameters of the side chains and pendant groups of the hosts as well as those of the guest atoms are larger than those of the atoms of the steroid ABCD fused-ring nuclei as is illustrated in Figs. 1(*a*)–(*c*). The side chain conformations of the host steroids, as defined by the torsion angles listed in Table 2, are similar in the two inclusion compounds that exhibit the extended conformation, minimising the curvature of the host molecule and thus minimising bilayer puckering. The MC(α) phase is not isostructural with the CA(α) phase and contains two crystallographically unique molecules in the asymmetric unit. These exhibit very different side chain conformations, molecule B having the extended conformation while molecule A exhibits a puckered side chain conformation resulting in increased curvature of the steroid molecule. The packing diagrams of the inclusion compounds viewed down [010] are presented as Figs. 2(*a*) and 2(*b*) and that of the MC(α) structure viewed down [001] as Fig. 2(*c*). Clearly the structures of the inclusion compounds approach being isostructural and exhibit the familiar motif of host bilayers held together by host–host hydrogen bonding of the hydrophilic sides of the steroid hosts. Unusually, there are no channels formed into which guest molecules pack and the acetonitrile molecules are held in cavities created by the packing of the pleated bilayers. There are no close contacts between host and guest.

The independent host molecules of the MC(α) phase with their significantly different conformations show very different hydrogen bonding schemes. Distances and angles defining the hydrogen bond schemes are detailed in Table 3 and the differences for MC hosts A and B are illustrated in Fig. 3. A number of O–H · · · O interactions that may appear possible from this diagram [such as that between O(29B) and O(26B)] are at best very weak interactions with poor O–H · · · O geometry and long O · · · O distances. This contrasts strongly with the CA(α) structure in which there is a single unique host molecule in the asymmetric unit and a very different hydrogen bonding scheme. It is of particular interest that the hydrogen bonding potential of the CA molecule is fully realised in the α phase while that of the MC host molecule is not, a number of potentially hydrogen bonded groups only being involved in very weak interactions. The hydrogen-bonding schemes for the two inclusion compounds are similar to those found in many of the CA tubulate clathrate inclusion compounds. The host–host hydrogen bonding system, which facilitates formation of bilayers, is disrupted in the compound with the methyl ester host as O(28) no longer participates in the hydrogen bonding scheme. The acid host bilayer structure is stabilised by the hydrogen bonding system: O(28)–H(28O) · · · O(29)–H(29O) · · · O(25)–H(25O) · · · O(26)–H(26O) · · · O(27) while the scheme of the ester host hydrogen bonding is O(26)–H(26O) · · · O(25)–H(25O) · · · O(29)–H(29O) · · · O(27). The difference in the hydrogen bonding order is not necessarily due to the intervention of the ester group as similar behaviour has been noticed in otherwise isostructural compounds.[17]

It might be predicted that the loss of a hydrogen bond would lead to the lowering of the potential barrier to release of the volatile guest with concomitant collapse of the structure; however this is not borne out by lowered guest release temperature in MCCN as measured by rising temperature DSC. Thermograms of each of the inclusion compounds are illustrated in Fig. 4. While large single crystals of the MCCN compound show a single endotherm in the DSC trace, finely powdered MCCN indicates a well-defined guest loss endotherm followed by the host melt (dotted line). This disparity may be explained by observation of the behaviour of varying particle sizes of MCCN under similar heating rates using a hotstage microscope. Large single crystals of MCCN melt at the temperature that guest loss occurs and recrystallisation is only observed under slow heating rates or after added nucleation sites are provided by scratching. Very small particles, on the other hand, do not melt at the temperature of the first endotherm (and guest loss event) although evolution of gas, due to guest vapours, is observable if the particles are submerged in a droplet of silicone oil. The CACN compound always exhibits both guest loss and host melt endotherms.

When exposed to acetonitrile vapours, dry, powdered CA and MC spontaneously react to form the 1 : 1 inclusion compounds. The adsorption isotherms of CA and MC with acetonitrile at 20 °C and acetonitrile vapour pressure 78 mmHg are presented as Fig. 5. Surprisingly the reaction: $MC_{(s)} + CH_3CH_{(g)} \rightleftharpoons MC{\cdot}CH_3CH_{(s)}$ proceeds more rapidly than: $CA_{(s)} + CH_3CN_{(g)} \rightleftharpoons CA{\cdot}CH_3CN_{(s)}$ at this temperature with a half life of *ca.* 8.5 minutes for MCCN formation and *ca.* 26

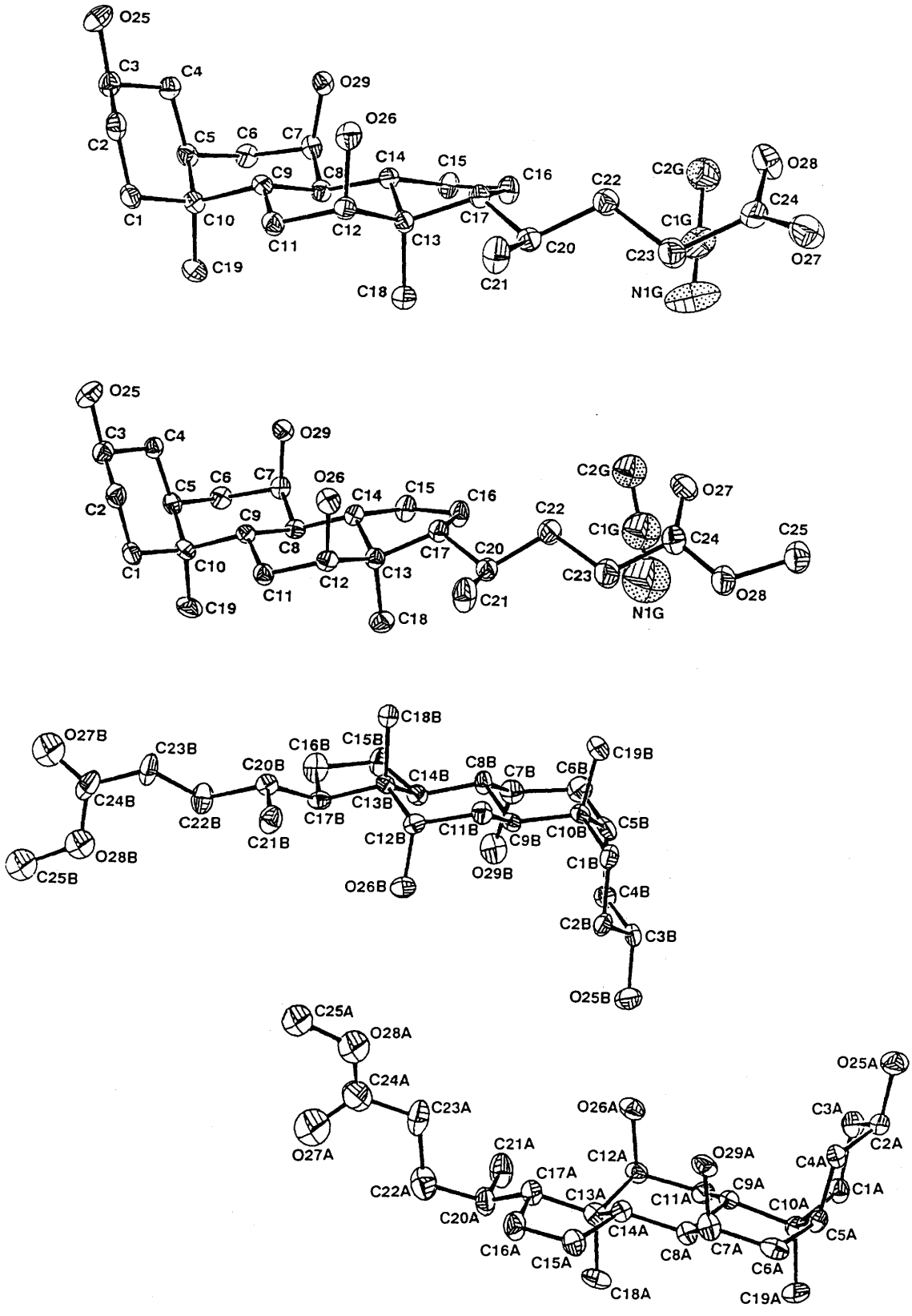

Fig. 1 ORTEP diagrams drawn at 30% enclosure ellipsoids for CACN, MCCN and MC(α) showing atomic numbering. Guest atoms are speckled

minutes for CACN formation. In both cases the reaction appears to follow a first rate law.

In an attempt to understand the large difference in reactivity towards acetonitrile of these very similar hosts we investigated the kinetics of desorption of acetonitrile from each inclusion compound. Desorption reactions were carried out over a range of temperatures as described in the experimental section and values of k thus obtained are presented in Table 4. Arrhenius plots for the appropriate mechanisms of guest release and structural collapse to the α-form are presented as Figs. 6(*a*) and (*b*). It is apparent, from the straight line nature of the plots that the guest release reaction: $HG_{(s)} = H_{(s)} + G_{(g)}$ for each complex

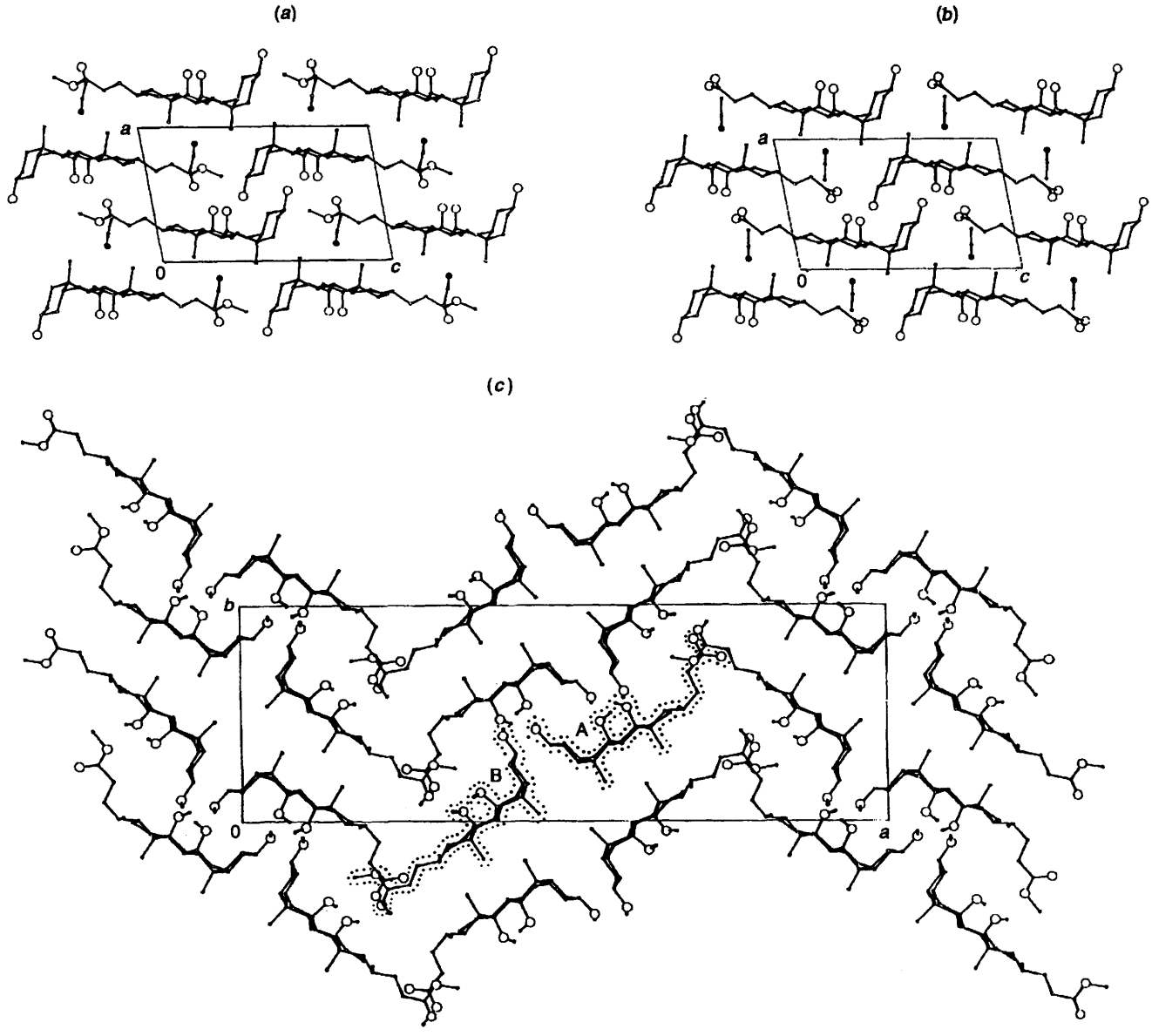

Fig. 2 Packing diagrams of CACN and MCCN viewed down [010] (*a*) and (*b*) and of MC(α) viewed down [001] (*c*). The two crystallographically independent host molecules of MC(α) are highlighted with dotted outlines and labelled A and B and nitrogen atoms are depicted as filled circles.

is isokinetic over the temperature ranges studied. Desorption of acetonitrile from CACN with concomitant collapse to the CA(α) structure may be best described by the Avrami–Erofeev equation derived to model 2-dimensional nucleation and growth of the product phase, which is characterised by sigmoidal α *versus* time curves. Decomposition of MCCN is best described by a rate law based on 3-dimensional diffusion of guest away from the desorption site through the burgeoning MC(α) layer. Estimates of activation energy, E_a, and the preexponential factor, A, for each possible model are presented as Table 5. While the terms E_a and A as derived in the Arrhenius equation are of dubious physical significance in the description of solid phase reactions they nonetheless serve as empirical descriptors of the reaction under consideration and are thus useful as comparative quantities. The values of the preexponential factors are of similar orders for each reaction implying that contributions to the constants describing vibration as well as other factors are similar for both reactions. Note that the 'activation energy' for the decomposition of MCCN is significantly larger than that for the decomposition of CACN. This is initially surprising as the structures are virtually isostructural except that that of CACN has the added stabilisation of one extra hydrogen bond per host molecule. Thus the ester MC reacts with acetonitrile more rapidly than the free acid CA and MCCN shows a higher energy barrier to desorption of the guest than CACN. This is contrary as one might expect the packing energy of MCCN to be lower than that of CACN allowing ready collapse of the structure resulting in a lower E_a value.

In an attempt to reconcile the kinetic data with structure we carefully considered similarities and differences in the structures of phases involved in the reaction: $HOST{\cdot}CH_3CN_{(s,\beta)} = HOST_{(s,\alpha)} + CH_3CN_{(g)}$ hoping that this might supply the reason for the apparently anomalous fact that the inclusion compound less stabilised by hydrogen-bonding compound is *more* readily formed and *less* readily decays. It is immediately obvious that the α structure of the MC host allows for fewer and weaker hydrogen bonds than that of CA. In fact the potential of certain of the hydroxy and ester groups to form hydrogen bonds remains unfulfilled. In an attempt to quantify the *difference* in hydrogen bond stabilisation between the two α phases we calculated values of the atom–atom potential functions for all hydrogen bonds in each structure and expressed these per host molecule. (Data for calculation of

Table 3 Hydrogen bonding schemes

	O···O/Å	H···O/Å	O–H···O/°	H···O–C/°		$U_{hb}(r)$/kJ mol^{-1}
CACN						
O(28)–H(28O)···O(29)[a]	2.629(5)	1.70(6)	156(3)	139(2)		−8.81
O(29)–H(29O)···O(25)[b]	2.714(7)	1.77(4)	162(5)	124(2)		−14.42
O(25)–H(25O)···O(26)[b]	2.750(6)	1.83(4)	157(3)	115(2)		−14.49
O(26)–H(26O)···O(27)[c]	3.015(7)	2.14(4)	149(2)	138(1)		−4.81[k]
						−42.53
MCCN						
O(26)–H(26O)···O(25)[d]	2.794(7)	1.83(4)	174(4)	122(2)		−16.36
O(25)–H(25O)···O(29)[d]	2.857(9)	1.93(4)	157(4)	124(3)		−11.18
O(29)–H(29O)···O(27)[e]	2.918(6)	1.99(6)	156(4)	147(2)		−7.94[k]
						−35.48
MC(α)						
O(25A)–H(5AO)···O(29A)[f]	3.028(10)	2.10(4)	160(9)	129(3)		−6.69
O(29A)–H(9AO)···O(25B)[g]	2.830(9)	1.90(2)	160(4)	112(1)		−13.49
O(25B)–H(5BO)···O(26A)[f]	2.730(9)	1.78(3)	174(10)	119(4)		−17.08
O(26A)–H(6AO)···O(25A)[f]	2.884(9)	1.93(2)	178(9)	135(3)		−11.58
O(26B)–H(6BO)···O(27B)[h]	2.945(11)	2.05(5)	155(9)	146(3)		−6.65[k]
O(29B)–H(9BO)···O(26B)[i]	3.254(10)	2.82(7)	141(8)	114(2)		−1.30
O(29B)–H(9BO)···O(28A)[j]	3.612(10)	2.50(8)	136(8)	134(3)		−0.32
					(2 hosts)	−57.11
					(1 host)	−28.56
CA(α) (Miki *et al.*[25])						
O(28)–H(28)···O(26)	2.634	1.68	173	149		−8.81
O(26)–H(26)···O(25)	2.723	1.80	174	122		−14.42
O(25)–H(25)···O(29)	2.774	1.88	171	126		−14.97
O(29)–H(29)···O(27)	2.857	1.98	169	150		−4.81[k]
						−43.01

[a] $-x-1, y-\frac{1}{2}, -z-2$. [b] $-x-1, y+\frac{1}{2}, -z-1$. [c] $-x-1, y+\frac{1}{2}, -z-2$. [d] $-x-2, y-\frac{1}{2}, -z-2$. [e] $-x-2, y+\frac{1}{2}, -z-1$. [f] $-x+2, -y, z$. [g] $-x-2, -y, z+1$. [h] $-x+1\frac{1}{2}, y-\frac{1}{2}, -z+1$. [i] $-x+2, -y, z-1$. [j] $x, y, -1+z$. [k] Carbonyl oxygen atom, expect sp^2 hybridisation; $\chi_O = 120°$.

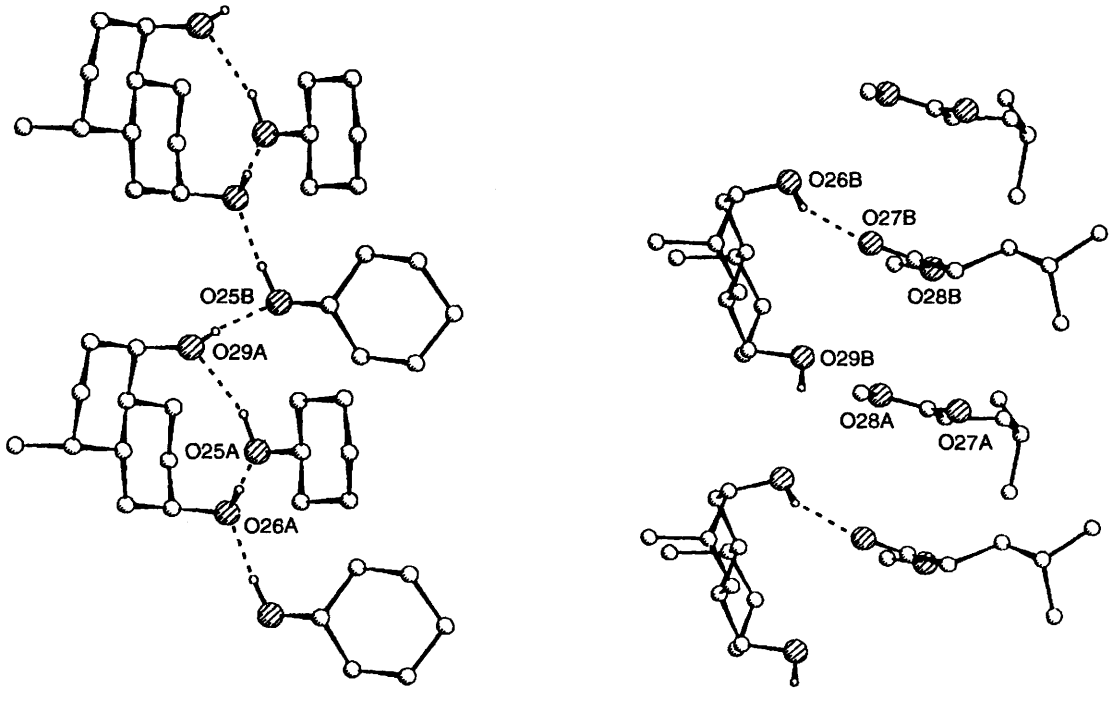

Fig. 3 The two separate hydrogen-bonding schemes of MC(α) viewed normal to [001]

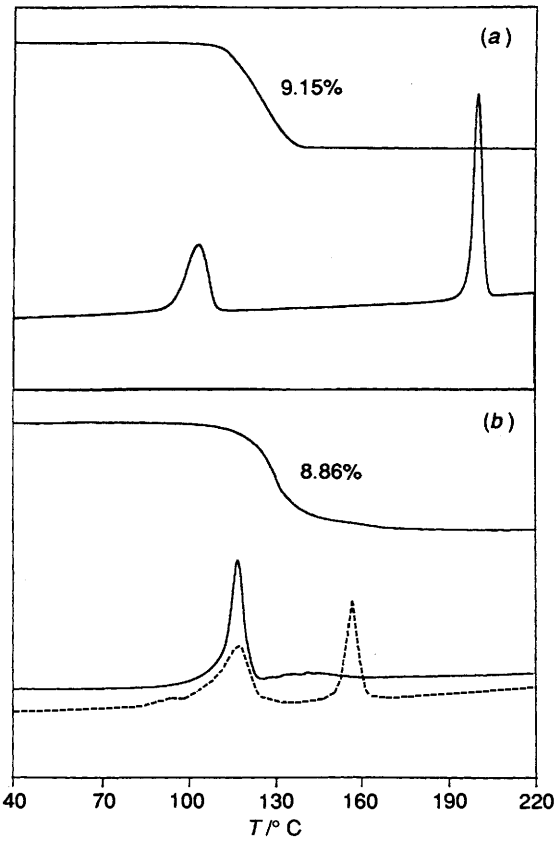

Fig. 4 Programmed rising temperature TG and DSC curves for (*a*) CACN and (*b*) MCCN. The DSC trace of large single crystals of MCCN is represented by a solid line while that of the powder is drawn as a broken line.

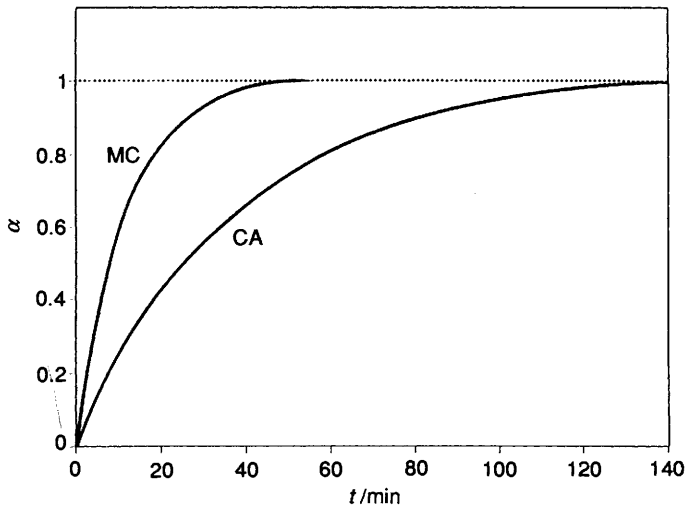

Fig. 5 α *versus* time curves for the absorption of acetonitrile by MC and CA at 20 °C

CA(α) atom–atom potentials were derived from the structure by Miki *et al.*[25]) We used a modified form of the Lennard–Jones potential function for non-bonded interactions between pairs of atoms: where the coefficients A and C are as modified by Vedani

$$E_{hb} = (A/r^{12}{}_{H\cdots O} - C/r^{10}{}_{H\cdots O}) + \cos^2(\theta_{O\text{-}H\cdots O})\cos^2(\chi_{H\cdots O\text{-}C} - \chi_0)$$

and Dunitz,[26] r is the distance between the donor hydrogen atom and the acceptor oxygen atom and θ and χ are the angles between donor O, donor H and acceptor O and between donor H, acceptor O and acceptor C respectively. These angles

Table 4 Rate constants for isothermal decompositions of CACN and MCCN

	T/°C	$k/10^{-3}$ min^{-1}	r^2
CACN	85	1.507(2)	0.9989
A2 rate law	85	1.869(5)	0.9947
	88	2.939(7)	0.9954
	90	3.63(1)	0.9922
	92	8.81(2)	0.9952
	94	15.51(6)	0.9943
	96	28.9014)	0.9946
	97	23.57(8)	0.9938
	98	51.21(2)	0.9946
	99	55.22(2)	0.9819
	100	38.0(2)	0.9886
	102	88.1(9)	0.9847
	103	138(1)	0.9902
	105	152(1)	0.9909
	107	181(2)	0.9892
	108	249(3)	0.9894
	110	337(4)	0.9900
	112	529(3)	0.9975
	115	711(6)	0.9977
MCCN	85	0.444(1)	0.9995
D3 rate law	87	0.829(1)	0.9997
	90	1.83(1)	0.9968
	93	3.86(3)	0.9900
	94	6.59(11)	0.8768
	95	7.11(2)	0.9953
	97	12.02(3)	0.9975
	98	17.81(4)	0.9975
	100	21.9(1)	0.9960
	100	23.7(1)	0.9963

Table 5 Kinetic data derived for desorption reactions

	CACN	MCCN
Rate law	A2	D3
α range	0.05–0.95	0.05–0.95
ln A	75.5(3)	88.6(1)
E_a/(kJ mol^{-1})	244(9)	287(8)
r^2	0.9788	0.9935

are quoted in Table 3 and describe the geometry of the hydrogen bond. In the 'best case' one would expect the angle O–H · · · O to approach 180° (a linear H-bond) while the angle H · · · O–C will depend on the hybridisation at the C atom and will thus ideally be either 109.5 or 120° (the quantity χ_0 accounts for this ideality). The modification to take into account the geometry of the lone pair orbitals at the *acceptor* atom (the third term) is as suggested by Vedani and Dunitz[26] and is important in correctly weighting the approach to ideal geometry of the hydrogen bond. Values for the hydrogen bond potentials are quoted in Table 3. It becomes clear from the total hydrogen-bonded potential per host molecule that formation of CA(α) is a far more favourable reaction than formation of MC(α). If the differences in hydrogen-bonded potentials between reactant and product species are computed instead, the same trend is noted. While the favourable interactions occurring upon formation of hydrogen bonds are by no means the only energy considerations it is to be expected that all other terms will be of similar magnitude in the inclusion compounds given that these are isostructural, exhibit the same stoichiometry and lack of host:guest interactions. The structures of CA(α) and MC(α) are not isostructural and the hydrogen bonded potential of CA(α) is larger than that of MC(α). Consideration of the relative melting points of the host compounds (MC melt onset 150 °C, CA melt onset 200 °C) reveals that the sum of all factors such dispersion forces, packing

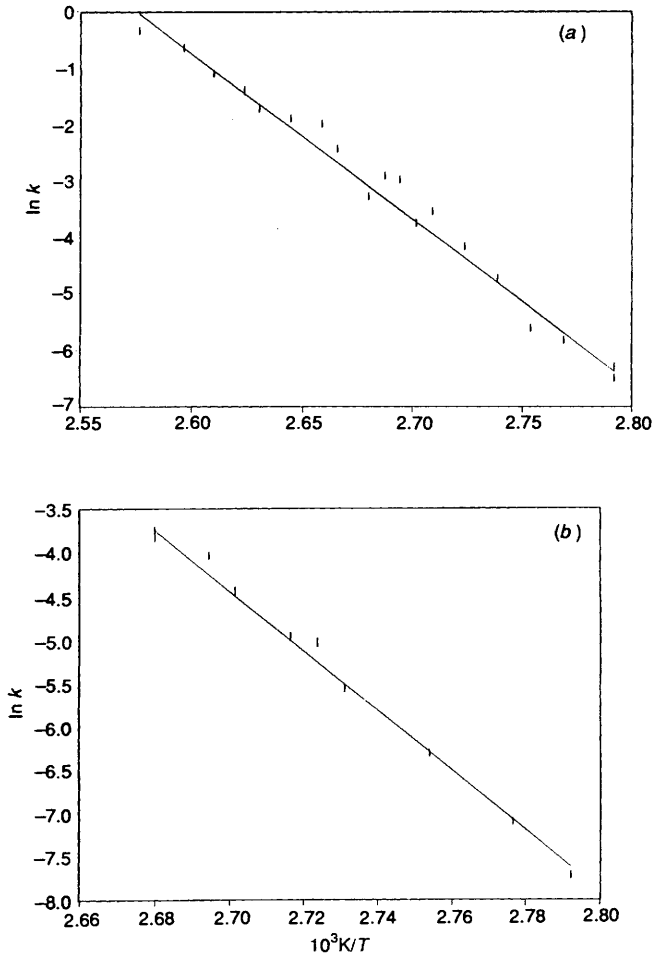

Fig. 6 Arrhenius plots for the appropriate mechanisms of decay of (*a*) CACN {A2 rate law: $kt = [-\ln(1-\alpha)]^{\frac{1}{2}}$} and (*b*) MCCN {D3 rate law: $kt = [1-(1-\alpha)^{\frac{1}{3}}]^2$}

efficiency and hydrogen bonding, reflect the trend in hydrogen bonding potential.

Thus we suggest that the lower energy requirements for overcoming hydrogen-bonded and other interactions in the MC(α) phase and the greater gain in hydrogen bonded potential of CA(α) defines the relative rates of formation, and energy barrier to decomposition of the inclusion compounds with acetonitrile.

Acknowledgements

The author wishes to thank Professors M. R. Caira and L. R. Nassimbeni for fruitful discussion and constructive criticism.

References

1 J. L. Scott, unpublished results.
2 F. Toda, K. Tanaka and A. Skikawa, *J. Chem. Soc., Chem. Commun.*, 1987, p. 279.
3 R. P. Townsend and M. F. M. Post, in *Introduction to Zeolite Science and Practice*, ed. H. van Bekkum, E. M. Flanigan and J. C. Jansen, Elsevier, Amsterdam, 1991.
4 R. M. Barrier, in *Zeolites and Clay Minerals as Sorbents and Molecular Sieves*, Academic Press, London, 1978.
5 J. Lipkowski, in *Inclusion Compounds*, vol. 1, ed. J. L. Atwood, J. E. D. Davies and D. D. MacNicol, Academic Press, London, 1984.
6 J. Votnisky, J. Kalonsova, I. Benes, J. Bandysova and V. Zima, *J. Inclusion Phenom. Mol. Recog. Chem.*, **15**, 1993, 71.
7 A. Ehlen, C. Wimmer, E. Weber and J. Bargon, *Angew. Chem., Int. Edn. Engl.*, 1993, **32**, 110.
8 L. J. Barbour, M. R. Caira and L. R. Nassimbeni, *J. Chem. Soc., Perkin Trans. 2*, 1993, 2321.
9 D. R. Bond, L. Johnson, L. R. Nassimbeni and F. Toda, *J. Solid State Chem.*, 1991, **92**, 68.
10 P. L. Johnson and J. P. Schaeffer, *Acta. Crystallogr., Sect. B.*, 1972, **28**, 3083.
11 E. L. Jones and L. R. Nassimbeni, *Acta. Crystallogr., Sect. B*, 1990, **46**, 399.
12 K. Miki, A. Masui, N. Kasai, W. G. M. Shibakami, K. Takamoto and M. Miyata, *Acta. Crystallogr., Sect. C*, 1992, **48**, 503.
13 K. Nakano, K. Sada and M. Miyata, *Chem. Lett.*, 1994, 137.
14 M. R. Caira, L. R. Nassimbeni and J. L. Scott, *J. Chem. Soc., Chem. Commun.*, 1993, 612.
15 K. Miki, A. Masui, N. Kasai, M. Miyata, M. Shibakami and K. Takemoto, *J. Am. Chem. Soc.*, 1988, **110**, 6594.
16 M. Shibakami and A. Sekiya, *J. Chem. Soc., Chem. Commun.*, 1994, 429.
17 M. R. Caira, L. R. Nassimbeni and J. L. Scott, *J. Chem. Soc., Perkin Trans. 2*, 1994, 623.
18 M. R. Caira, L. R. Nassimbeni and J. L. Scott, *J. Chem. Crystallogr.*, 1994, **24**, 783.
19 K. Miki, N. Kasai, M. Shibakami, K. Takemoto and M. Miyata, *J. Chem. Soc., Chem. Commun.*, 1991, 1757.
20 G. M. Sheldrick, SHELX-86, *Crystallographic Computing 3*, ed. G. M. Sheldrick, C. Kruger and R. Goddard, Oxford University Press, 1985, 175.
21 G. M. Sheldrick, SHELX-76 *Program for Crystal Structure Determination*, University of Cambridge, Cambridge, UK, 1976.
22 G. M. Sheldrick, SHELXL-93: *A Program for Crystal Structure Determination, J. Appl. Crystallogr.*, 1993, in preparation.
23 M. E. Brown, in *Introduction to Thermal Analysis, Techniques and Applications*, Chapman and Hall, London, 1988.
24 L. J. Barbour, K. Achleitner and J. R. Greene, *Thermochimica Acta*, 1992, **205**, 171.
25 K. Miki, N. Kasai, M. Shibakami, S. Chirachanchai, K. Takemoto and M. Miyata, *Acta. Crystallogr., Sect. C*, 1990, **46**, 2442.
26 Angelo Vedani and Jack D. Dunitz, *J. Am. Chem. Soc.*, 1985, **107**, 7653.

Paper 4/04824E
Received 5*th August* 1994
Accepted 14*th November* 1994